Dynamic identification of a Mitsubishi PA-10 robotic manipulator

R. van der Aalst B.Sc.

DCT 2008.050

Traineeship report

Coach(es): Dr. Marcelo H. Ang Jr
(National University of Singapore)
Lim C.W. M.Eng.
(Singapore Institute of Manufacturing Technology)

Supervisor: Prof.dr. H. Nijmeijer
(Eindhoven University of Technology)

Technische Universiteit Eindhoven
Department Mechanical Engineering
Dynamics and Control Group

Eindhoven, April, 2008

Abstract

In this report the system parameters identification for a Mitsubishi PA-10 robotic manipulator is considered. The Singapore Institute of Manufacturing Technology has, in collaboration with the National University of Singapore, developed a specific method to do this system identification. This report focusses on using that identification method.

The main advantages of the method are that it consists of a structured procedure to follow so it is easily applied to different kind of robotic manipulators and furthermore no need of measured acceleration information is required.

Before the identification procedure can be used the full dynamic model of the robotic manipulator is derived. Reduction of system parameters is structurally applied because of the necessity to reduce system complexity if to be used for identification purposes.

The identification procedure is based on achieving a fully undamped system by using modeled friction compensation. Originally the friction compensation is done based on the assumption of viscous friction being dominantly present in the robotic joints. This does not result in undamped system behaviour. It is shown by means of experimental friction identification that Coulomb friction is significantly present in the robotic joints. Relating to this result the friction compensation model is expanded with Coulomb friction using experimentally identified parameter values obtained from a least-square fit through gathered data points. Despite using this expended friction model as compensation, the system is still effected by friction influences that remain because of the real friction deviating from the modeled friction. It is shown that this deviations between modeled, and thus compensated friction, and real friction result in specific system behaviour that is clearly not nicely undamped.

It is concluded that a friction model, gained by experimental means, can result in control improvements while used to compensate the friction but that it is not possible to succeed in obtaining a fully undamped system. There will always be deviations between the modeled friction used to compensate and the real friction present. Therefore the identification method should be regarded impractical and it can not be used to identify system parameters as supported by erroneous identification results.

Contents

Chapter 1

Introduction

Nowadays robotic manipulators take more and more a significant place in industry. They improve quality and safety while reducing costs and processing time in fully automated production lines. In these automated production lines robotic manipulators can perform a wide variety of tasks ranging from welding, cutting, bonding and painting to material handling. As research pushes performance limits more possibilities for application of robotic manipulators arise. A promising technique that is currently topic of many researches to achieve robotic control improvement is the usage of model-based control.

At the Singapore Institute for Manufacturing Technology (SIMtech) the robotic team is working on the implementation of force control on robotic manipulators. To achieve this, one of the major challenges is to implement such a model-based controller in a well-structured manner. This subgoal on its own, the implementation of model-based control, possesses challenges as describing the complete dynamic behaviour of the robot using a mathematical model. To be able to use such a mathematical model describing the robotic manipulator dynamics, it is necessary to know the values of all system parameters. The robotic manipulator used is a Mitsubishi PA-10 as visible in figure 1.1.

The specific objective of this research is defined as follows; describe the complete dynamics of the Mitsubishi PA-10 robotic manipulator and identify all unknown system parameters, used in the obtained dynamic model, by experimental means. To do this identification an experimental method as proposed by SIMtech[1][14] is applied.

This report is organized as follows. First, in Chapter 2, the robotic dynamics will be addressed using a mathematical model. Furthermore this model is prepared for usage in the experimental identification of unknown parameters. Before the experimental identification method is fully addressed in Chapter 4, some alternatives are briefly mentioned in Chapter 3. The theory of Chapter 4, regarding the identification experiment, is applied on the Mitsubishi PA-10. Chapter 5 presents and discusses the results of the experiment. Finally general discussion takes place in Chapter 6 followed by recommendations for future research progress.

[1] Developed in collaboration with the National University of Singapore (NUS).

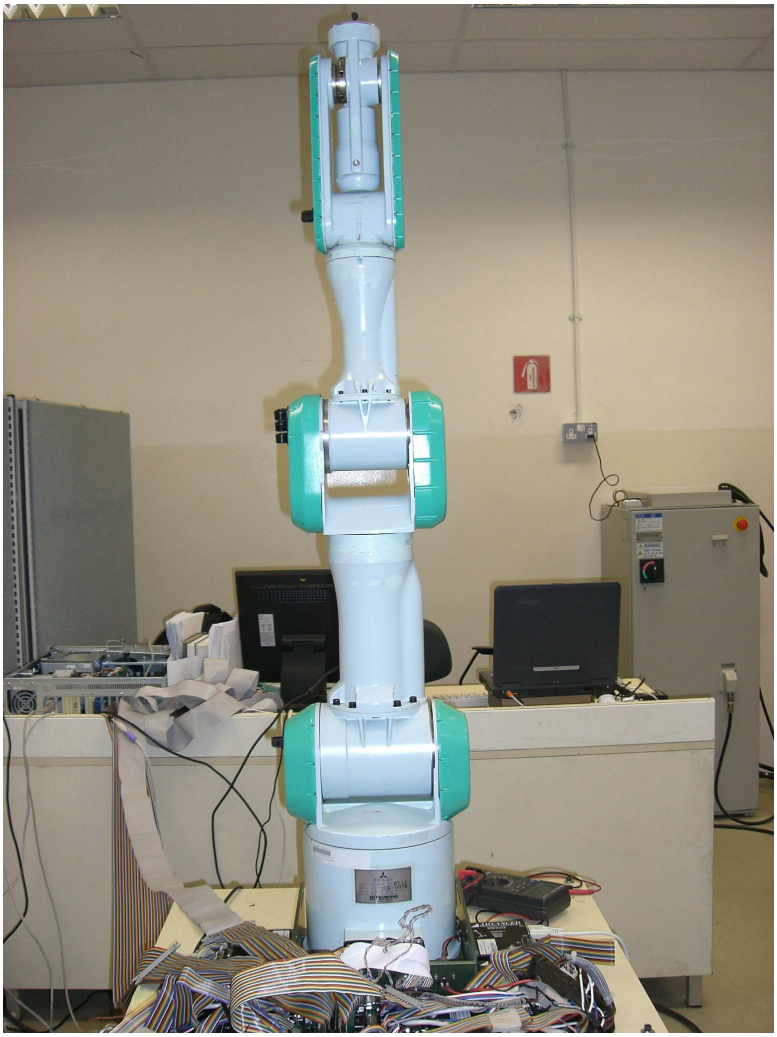

Figure 1.1: The Mitshubishi PA-10 robotic manipulator.

Chapter 2

Robot modeling

2.1 Introduction

The general objective of SIMtech is to implement model-based control. To make this possible a dynamic model has to be derived. After the general introduction of a Mitsubishi PA-10 robotic manipulator in section 2.2, some coordinate frame conventions are defined in section 2.3. In section 2.4 the equations of motion are stated. Finally the set of minimal inertial parameters in which the equations of motion can be expressed are determined in section 2.5, besides some other assumptions that simplify the model.

2.2 The Mitsubishi PA-10

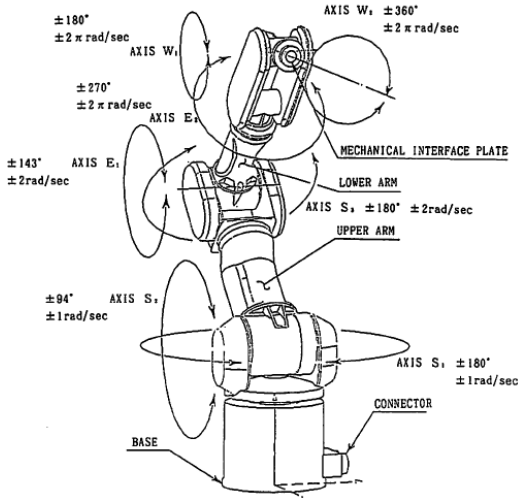

Figure 2.1: Graphical representation of the Mitshubishi PA-10 robotic manipulator [5].

The Mitsubishi PA-10 is a robotic manipulator as depicted in figure 2.1. It possesses seven degrees of freedom, thus a so-called shoulder, elbow and wrist are present. Indicated are the limits of the joint rotations and the maximum joint velocities.

2.3 Kinematics

To be able to describe the robotic kinematics a coordinate frame has to be assigned to each joint. The coordinate frame assignment as used throughout this report is visible in figure (2.2) and is conform the modified Denavit-Hartenberg (MDH) convention [1]. The corresponding MDH-parameters are listed in table 2.1 and according to the MDH convention defined as:

a_i The distance from z_i to z_{i+1} measured along x_i,

α_i The angle between z_i and z_{i+1} measured about x_i,

d_i The distance from x_{i-1} to x_i measured along z_i,

θ_i The angle between x_{i-1} and x_i measured about z_i,

where $i = 1, \ldots, 7$. Furthermore the frames are placed in such a way that a positive sensor feedback corresponds to the positive direction conform the MDH convention.

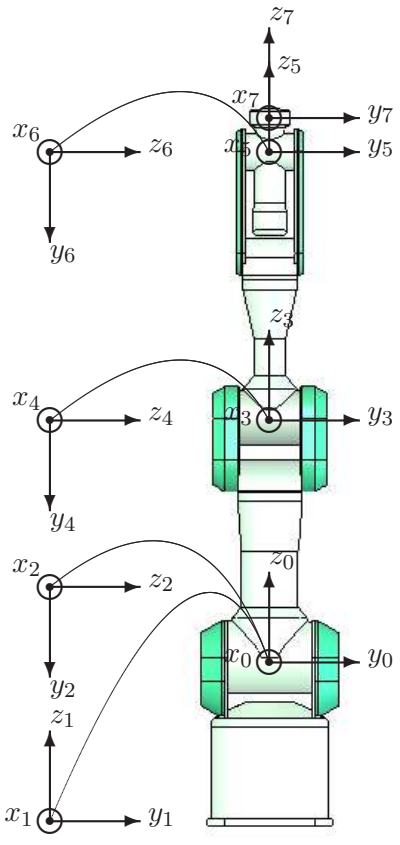

Figure 2.2: Links and frame assignment of the PA-10.

link i	a_i	α_i	d_i	θ_i
1	0	0	0	θ_1^*
2	0	-90	0	θ_2^*
3	0	90	d_3	θ_3^*
4	0	-90	0	θ_4^*
5	0	90	d_5	θ_5^*
6	0	-90	0	θ_6^*
7	0	90	d_7	θ_6^*

Table 2.1: Modified Denavit-Hartenberg parameters

Using this frame assignment the kinematic relation between frame i and frame $i+1$, and corresponding joints, is described with the following homogeneous transformation matrix:

$$\mathrm{T}_{i+1}^{i} = \begin{bmatrix} cos(\theta_i) & -sin(\theta_i) & 0 & a_i \\ sin(\theta_i)cos(\alpha_i) & cos(\theta_i)cos(\alpha_i) & -sin(\alpha_i) & -sin(\alpha_i)d_i \\ sin(\theta_i)sin(\alpha_i) & cos(\theta_i)sin(\alpha_i) & cos(\alpha_i) & cos(\alpha_i)d_i \\ 0 & 0 & 0 & 1 \end{bmatrix} \tag{2.1}$$

Furthermore the PA-10 is an open kinematic chain and therefore the forward kinematics can be computed as a product of homogenous transformations between circumjacent coordinate frames:

$$\mathrm{T}_{i}^{0} = \mathrm{T}_{1}^{0}\mathrm{T}_{2}^{1}\dots\mathrm{T}_{i}^{i-1} \tag{2.2}$$

2.4 Dynamic rigid-body modeling

A rigid-body model is used to describe the robot dynamics. The rigid-body model can be derived using the Euler-Lagrange formulation [1,2,3]. The general form of the model with friction included is as follows:

$$\tau(t) = D(q(t))\ddot{q}(t) + C(q(t), \dot{q}(t)) + h(q(t)) + \tau^f(t) \tag{2.3}$$

Where q is a vector representing the joint angles, $q = [\theta_1 ... \theta_7]^T$, and $\dot{q}$ and $\ddot{q}$ represent joint velocities and joint accelerations respectively. Furthermore $D(q(t))$ represents the inertia matrix and $C(q(t))$, $h(q(t))$ and $\tau^f(t)$ represent vectors that contain the Coriolis/centripetal, gravitational and friction forces respectively. The elements of inertia matrix $D(q(t))$ are defined as:

$$d_{j,k} = \sum_{i=\max(j,k)}^{7} \mathrm{Tr}\left[\left(\frac{\partial}{\partial q_k}\mathrm{T}_i^0\right) J_i \left(\frac{\partial}{\partial q_j}\mathrm{T}_i^0\right)^T\right] \tag{2.4}$$

and the elements of $C(q(t), \dot{q}(t)))$ are defined using *Christoffel* symbols:

$$c_j = \sum_{k=1}^{7}\sum_{l=1}^{7} c_{j,k,l}\dot{q}_k\dot{q}_l, \tag{2.5}$$

$$c_{j,k,l} = \sum_{i=\max(j,k,l)}^{7} \mathrm{Tr}\left[\left(\frac{\partial^2}{\partial q_k \partial q_l}\mathrm{T}_i^0\right) J_i \left(\frac{\partial}{\partial q_k}\mathrm{T}_i^0\right)^T\right] \quad j,k,l = 1,\dots,7 \tag{2.6}$$

Furthermore the gravitational effects are added in $h(q(t))$ as:

$$h_j = \sum_{i=j}^{7}\left(-m_i\mathbf{g}\left(\frac{\partial}{\partial q_j}\mathrm{T}_i^0\right) r_i\right) \quad j = 1,\dots,7 \tag{2.7}$$

Here m_i is the mass of the ith link, r_i contains the homogeneous coordinates of the center of mass of link i expressed in the ith coordinate frame:

$$r_i = [x_i\ y_i\ z_i\ 1]^T \tag{2.8}$$

and **g** represents a gravity vector $\mathbf{g} = [0\ 0\ -g\ 0]$ where $g = 9.8062 m/s^2$. J_i is the pseudo inertia tensor described as:

$$J_i = \begin{bmatrix} \frac{-I_{xx_i}+I_{yy_i}+I_{zz_i}}{2} & I_{xy_i} & I_{xz_i} & m_i x_i \\ I_{xy_i} & \frac{I_{xx_i}-I_{yy_i}+I_{zz_i}}{2} & I_{yz_i} & m_i y_i \\ I_{xz_i} & I_{yz_i} & \frac{I_{xx_i}+I_{yy_i}-I_{zz_i}}{2} & m_i z_i \\ m_i x_i & m_i y_i & m_i z_i & m_i \end{bmatrix} \tag{2.9}$$

Here I_{xx_i}, I_{yy_i} and I_{zz_i} denote the principal moments of inertia and I_{xy_i}, I_{yz_i} and I_{xz_i} the products of inertia for link i. Furthermore $m_i x_i$, $m_i y_i$ and $m_i z_i$ represent the first moment of link i. All expressed with respect to the ith coordinate frame as defined in the modified Denavit-Hartenberg convention.

2.5 Base parameter set

The derived dynamic model, equation (2.3), is because of its size very impractical to use for identification or real-time control purposes. To make is suitable the model size has to be reduced. It is well known that such a dynamic model, excluding friction, can be linearly expressed in its inertial parameters. Each link is described using 10 inertial parameters, so for the Mitsubishi PA-10 70 inertial parameters in total. However, some of these parameters have no effect on the dynamic model and others may appear in linear combinations. By eliminating the inertial parameters that have no effect on the dynamic model and by regrouping the linear combinations of the inertial parameters one can get a set of minimum inertial parameters, the base parameter set (BPS), that still fully describes the manipulators dynamics. To do this elimination and regrouping by hand is a very tedious and time-consuming operation. Furthermore it is not sure that the optimal solution of the BPS is obtained. Here a structured method is used as proposed by [15,16,17] to find the BPS.

2.5.1 Definition of the inertial parameters

Again m_i denotes the mass and $m_i x_i$, $m_i y_i$ and $m_i z_i$ the first moments of link i. The inertia tensor of link i about the origin of coordinate frame i is denoted as:

$$I_i^i = \begin{bmatrix} I_{xx_i} & I_{xy_i} & I_{xz_i} \\ I_{xy_i} & I_{yy_i} & I_{yz_i} \\ I_{xz_i} & I_{yz_i} & I_{zz_i} \end{bmatrix} \tag{2.10}$$

The inertial parameters of the ith link are collected in a vector X_i defined as:

$$X_i = [I_{xx_i}\ I_{xy_i}\ I_{xz_i}\ I_{yy_i}\ I_{yz_i}\ I_{zz_i}\ m_i x_i\ m_i y_i\ m_i z_i\ m_i]^T \tag{2.11}$$

Furthermore X becomes the (70 x 1) vector that contains all robot inertial parameters defined as:

$$X = \left[X_1^T\ X_2^T\ \dots\ X_n^T\right]^T \tag{2.12}$$

Because of equation (2.3), except for friction, being linear in its inertial parameters it can be linearly rewritten using the last definitions stated above as:

$$\tau(t) = H(q(t), \dot{q}(t), \ddot{q}(t))X + \tau^f(t) \tag{2.13}$$

where H is the regression matrix.

2.5.2 Elimination of inertial parameters

Let E denote the kinetic energy and U denote the potential energy of the system. Because of the linearity in inertial parameters these can be rewritten as:

$$E = \sum_{j=1}^{70} \frac{\partial E}{\partial X_j} X_j \tag{2.14}$$

$$U = \sum_{j=1}^{70} \frac{\partial U}{\partial X_j} X_j \tag{2.15}$$

Here X_j refers to the jth element of X.

If $\frac{\partial E}{\partial X_j} = 0$ and $\frac{\partial U}{\partial X_j} = constant$ then the corresponding X_j has no effect on $\tau(t)$ and is therefore not an element of the BPS. It can be eliminated by putting it to zero in equation (2.13).
In case of the PA-10 the following inertial elements satisfy these conditions and therefore can be eliminated, i.e. put to zero:

$$I_{xx_1},\ I_{xy_1},\ I_{xz_1},\ I_{yy_1},\ I_{yz_1},\ mX_1,\ mY_1,\ mZ_1,\ m_1,\ mZ_2,\ m_2 \tag{2.16}$$

2.5.3 Regrouping

The next step to reduce the number of elements of the BPS is to regroup elements that are linearly dependent. In case of the PA10 all joints are rotational and the inertial elements I_{yy_i}, mZ_i and m_i can be eliminated by regrouping them using the following relations, starting from the last link down to the first:

$$\left.\begin{array}{lcllll}
I_{xxR_i} & = & I_{xx_i} & -I_{yy_i} & & \\
I_{xxR_{i-1}} & = & I_{xx_{i-1}} & +I_{yy_i} & +2d_i mZ_i & +d_i^2 m_i \\
I_{yyR_{i-1}} & = & I_{yy_{i-1}} & +cos^2(\alpha_i) I_{yy_i} & +2d_i cos^2(\alpha_i) mZ_i & +(a_i^2 + d_i^2 cos^2(\alpha_i)) m_i \\
I_{zzR_{i-1}} & = & I_{zz_{i-1}} & +sin^2(\alpha_i) I_{yy_i} & +2d_i sin^2(\alpha_i) mZ_i & +(a_i^2 + d_i^2 sin^2(\alpha_i)) m_i \\
I_{xyR_{i-1}} & = & I_{xy_{i-1}} & +a_i sin(\alpha_i) mZ_i & +a_i d_i sin(\alpha_i) m_i & \\
I_{xzR_{i-1}} & = & I_{xz_{i-1}} & -a_i cos(\alpha_i) mZ_i & -a_i d_i cos(\alpha_i) m_i & \\
I_{yzR_{i-1}} & = & I_{yz_{i-1}} & +cos(\alpha_i) sin(\alpha_i) I_{yy_i} & +2d_i cos(\alpha_i) sin(\alpha_i) mZ_i & +d_i^2 cos(\alpha_i) sin(\alpha_i) m_i \\
mX_{R_{i-1}} & = & mX_{i-1} & +a_i m_i & & \\
mY_{R_{i-1}} & = & mY_{i-1} & -sin(\alpha_i) mZ_i & -d_i sin(\alpha_i) m_i & \\
mZ_{R_{i-1}} & = & mZ_{i-1} & +cos(\alpha_i) mZ_i & +d_i cos(\alpha_i) m_i & \\
m_{R_{i-1}} & = & m_{i-1} & +m_i & &
\end{array}\right\} \tag{2.17}$$

So the subscript R denotes a replacement for the original inertial parameter and represents a group of original inertial parameters. The original inertial elements that are regrouped to such a replacement can be put zero in (2.13). With the MDH parameters as given in table 2.3 the regrouping relations for each specific joint can be calculated as presented in appendix (A).

The remaining elements in the BPS for each link then become:

Link 7: $I_{xxR_7},\ I_{xy_7},\ I_{xz_7},\ I_{yz_7},\ I_{zz_7},\ mX_7,\ mY_7$

Link 6: $I_{xxR_6},\ I_{xy_6},\ I_{xz_6},\ I_{yz_6},\ I_{zzR_6},\ mX_6,\ mY_{R_6}$

Link 5: $I_{xxR_5},\ I_{xy_5},\ I_{xz_5},\ I_{yz_5},\ I_{zzR_5},\ mX_5,\ mY_{R_5}$

Link 4: $I_{xxR_4},\ I_{xy_4},\ I_{xz_4},\ I_{yz_4},\ I_{zzR_4},\ mX_4,\ mY_{R_4}$

Link 3: $I_{xxR_3},\ I_{xy_3},\ I_{xz_3},\ I_{yz_3},\ I_{zzR_3},\ mX_3,\ mY_{R_3}$

Link 2: $I_{xxR_2},\ I_{xy_2},\ I_{xz_2},\ I_{yz_2},\ I_{zzR_2},\ mX_2,\ mY_{R_2}$

Link 1: I_{zzR_1}

The last step is to detect the existence of supplementary combinations for link 1 to 7, where link k denotes the first link for which holds: $\frac{\partial E}{\partial X_j} \neq 0$ and $\frac{\partial U}{\partial X_j} \neq constant$ for all the ten inertial parameters corresponding to that specific link. No supplementary regrouping is possible though.

So by using elimination and regrouping the number of inertial elements that describe the dynamic model is reduced from 60 to a BPS of 43. Expressing (2.13) using the BPS elements gives:

$$\tau(t) = H_{bps}(q(t), \dot{q}(t), \ddot{q}(t))X_{bps} + \tau^f(t) \tag{2.18}$$

Where X_{bps} is a (43 x 1) vector of the BPS elements and H_{bps} contains the collomns of the original H that correspond to the original elements in X that have now become part of the base parameter set X_{bps}.

To guarantee that our reduced model is correct and still represents the original system as described in (2.3) it is verified using a robotic model made in the Robotic Toolbox [4]. From this toolbox it is known that it gives reliable and accurate results.

2.6 Friction modeling.

The last element modeled in equation (2.3), $\tau^f(t)$, is to include the influence of friction forces. Friction is a very complex issue on its own and the emphasis of this report is initially on the identification of the inertial parameters. Later however, while describing experimental results (Chapter 5), the influence of friction becomes significant. Several general friction models will be used throughout this report. Despite the fact that the used models here are generally known in common engineering practice there is a large variety in terminology. The following definitions represent the terminology and corresponding mathematical formulas for the several friction models as used throughout this report [1]:

Coulomb friction: [figure 2.3] This friction component delivers a force when joint velocity is present, $\dot{q} \neq 0$. The applied force has opposite sign to the velocity direction and the magnitude

[1] Note that the direction of the force in the figures representing friction models is opposite from the force direction as really experienced by the joints. The reason for this is that in the model, equation (2.3), the friction forces are already translated to the right-hand sight.

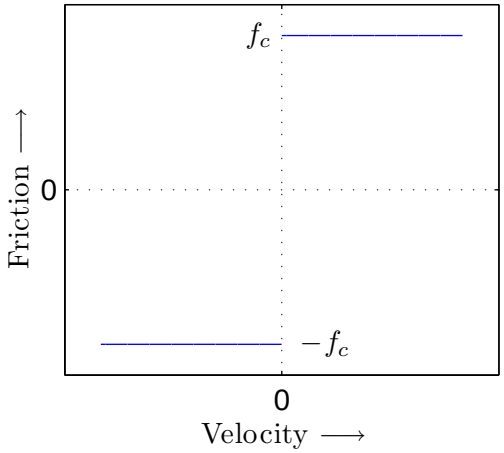

Figure 2.3: Coulomb friction.

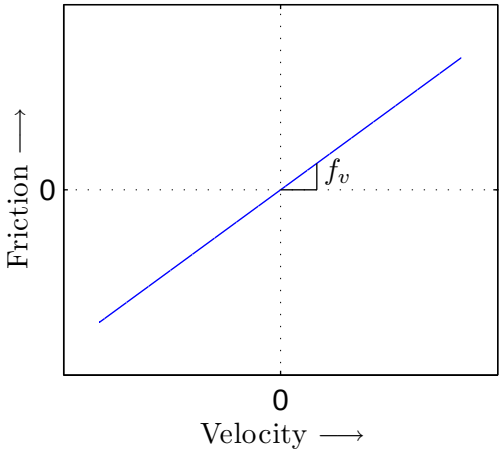

Figure 2.4: Viscous friction.

of the force is independent of the velocity magnitude. The equation used to represent Coulomb friction is as follows:

$$\tau_c^f(t) = f_c \text{sign}(\dot{q}) \tag{2.19}$$

Viscous friction: [figure 2.4] Similar to the Coulomb friction the viscous friction force is only present in case of joint velocity, $\dot{q} \neq 0$. The applied force is linear proportional to the magnitude of the velocity. Again the force the joint experiences has opposite sign of the velocity. The equation used to represent viscous friction is as follows:

$$\tau_v^f(t) = f_v \dot{q} \tag{2.20}$$

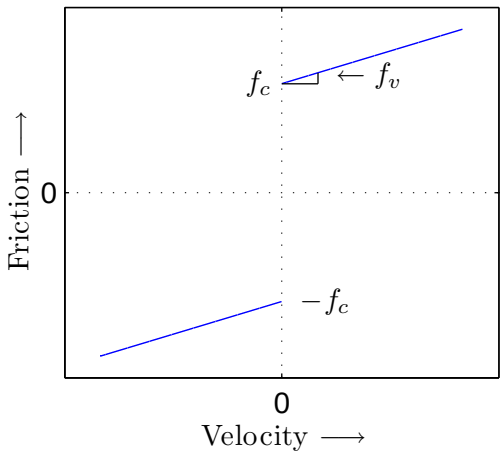

Figure 2.5: Coulomb and viscous friction combined.

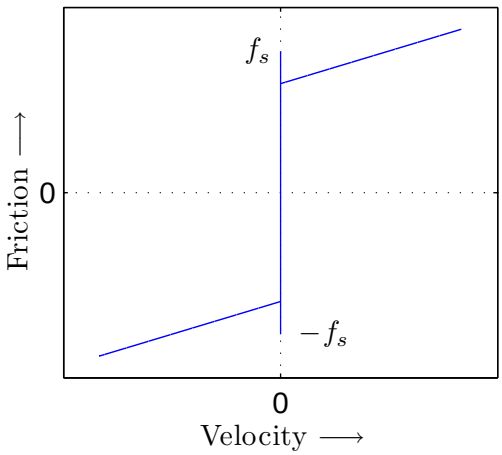

Figure 2.6: Coulomb and viscous friction with added static friction.

Static friction: [figure 2.6] In contrast to the Coulomb and viscous friction, that are only present in case of velocity being present, this friction delivers a force only at zero velocity. The static friction represents a force that has to be overcome by an initial force to initiate velocity. It is

opposite to the force initially applied and disappears as the joint has overcome the static friction value f_s, that is the joint breaks away and possesses a velocity.

Stribeck friction: A friction phenomenon that occurs in the low velocity region. This phenomenon is responsible for a nonlinear effect that decreases the friction force in the specific region till viscous friction dominates. However, as mentioned before, the main emphasis of this report is not on detailed friction identification and throughout this report the nonlinear phenomena that occur in the friction force because of the Stribeck effect are neglected. This is a reasonable assumption for the research done here because first of all it only effects the low velocity region and secondly detailed friction identifications done at Mitsubishi PA-10 robots have shown that the presence of the Stribeck effect is not really significant [18,19].

In practice the friction models described above are not stand-alone but occur all together in the robot joints. One of the friction combinations that is used throughout this report is the combination of Coulomb friction with viscous friction. So obvious this model becomes:

$$\tau_{vc}^{f}(t) = f_v\dot{q} + f_c\text{sign}(\dot{q}) \tag{2.21}$$

The corresponding friction graph is visible in figure (2.5)

Chapter 3

Literature review

3.1 Introduction

To implement model based control using an accurate dynamic model it is necessary to know all the dynamic parameters. The dynamic model parameters as provided by the manufacturer are insufficient. To acquire the unknown dynamic parameter values, identification experiments are necessary. SIMtech has already proposed such an experimental method as described in the next Chapter. Although this paper focuses on the use of that proposed method this Chapter briefly mentions other identification procedures for completeness.

3.2 Some available identification methods

The most straightforward identification method, regarding mass and inertia properties, would be dismantling the robotic manipulator. However, in most cases this is not a realistic option because of the manipulator's complexity. Another obvious method that is mentioned several times in literature [6,7,8] is the use of CAD drawings. This is not attractive though because robot manufacturers do not provide these drawings for all parts of the robot and it will give approximate values of which the accuracy is doubtful [7]. Other identification methods are known to make use of modal analysis [8] or frequency spectrum analysis [9].

However, most literature encountered during browsing describe slight variations on the following general procedure [7]:

- The dynamic model of the robot manipulator is derived in symbolic form.
- The minimal set of, to be identified, dynamic parameters that still fully describes the manipulator dynamics, i.e. the base parameter set, is determined.
- Model simplifications are done by reasonably neglecting the contribution, for example because of the manipulator's structure, of certain parameters.
- Specific trajectories are determined to gain a set of experimental data that optimizes the identification result.
- Finally the required values of the dynamic parameters are obtained by applying a suitable estimation algorithm.

Differences in the general procedure can be found in defining optimized trajectories and estimation algorithms but are mainly found in the use of different dynamic models for use of identification. Three models are commonly mentioned. First the so called explicit dynamic model, a dynamic model which depends on the joint acceleration and needs an explicit differentiation of the velocity. The main disadvantage of this is the introduction of noise in the signal by differentiation of the velocity to end up with the acceleration. Secondly a model that avoids this disadvantage is a model that differentiates a function of the velocity, the so called implicit dynamic model. However, the computational burden of this implicit model is much higher because of a complicated expression and no improvement in identification can be noticed [10]. The last method that gets a lot of attention in research literature is the use of a power model, which expression is obtained from rewriting an energy model in a differential form. The main advantage here is not the necessity to use acceleration information. The use of a power model receives positive criticism because of its simplicity and accuracy [10,11].

The above approaches suffer however from an important drawback [12]; they depend on torque information gained from actuator current measurements. The real torque applied to the joint deviates from the used measured torque information because of friction influences and limited precision of the actuator torque constants. An alternative model combines this internal measured information with externally gained information of the reaction forces and torques on the robotic manipulator's bedplate. This is measured by means of an external force/torque platform and thus totally independent of internal torques such as joint friction, allowing an accurate estimate of the inertial parameters. However, it must be noted that if the researcher is also interested in identifying joint friction parameters then a dynamic model that combines internal and external information is obviously a necessity. Such a combined model results in only a slight increase of the number of model parameters to be identified but a considerable increase of the number of force/torque data involved [12]. A obvious disadvantage is the addition of an external platform to the robotic manipulator to be able to measure reaction forces/torques. This is not a likely option in an industrial environment.

Despite this range of research methods, experimental identification of dynamical robotic manipulator parameters remains an active research topic for use in model-based control applications. Although almost all papers show control improvement by experimental means when identified parameters are used, no consensus is reached yet [13]. For exactly the same robotic manipulator very different identified values exist([note; after expressing with use of the same definitions]). This deviation in identified results leaves the possibility of trying other methods to identify dynamical parameters for use in model-based control.

SIMtech has, in cooperation with the National University of Singapore (NUS), developed an identification method that is simple and straightforward with the main advantage of not using acceleration information [14]. Here, for identifying system parameters of the Mitsubishi PA-10 robotic manipulator, this proposed method is used. In the next Chapter the theory of the identification method will be explained, later in Chapter 5 experimental results will be shown and commented on.

Chapter 4

Experimental identification of the inertial parameters

4.1 Introduction

To make the implementation of model based control possible it is necessary to know the values of the inertial parameters. The values of the link masses and their center of masses are supplied by the manufacturer Mitsubishi [5]. The inertias tensor elements are not known though. They should be identified by experimental means. In section 4.2 a last model simplification is done to reduce the number of unknowns that have to be experimentally determined. In section 4.3 the experimental method to determine the unknown inertial parameters is described.

4.2 Model reduction

To reduce the number of unknowns in the BPS the assumption is made that the robotic links are perfectly symmetric. In that case the inertia tensor expressed with respect to a frame that coincides with the center of mass of link i becomes[2,3]:

$$I_i^{cm_i} = \begin{bmatrix} I_{xx_6}^{cm} & 0 & 0 \\ 0 & I_{yy_6}^{cm} & 0 \\ 0 & 0 & I_{zz_6}^{cm} \end{bmatrix} \tag{4.1}$$

So the products of inertia become zero. If this result is translated to a inertia tensor which is with respect to coordinate frame i of link i, instead of the frame in the center of mass, then the values of those diagonal elements are known because of the *Steiner* translation formula:

$$I_i^i = \begin{bmatrix} I_{xx_i} & I_{xy_i} & I_{xz_i} \\ I_{xy_i} & I_{yy_i} & I_{yz_i} \\ I_{xz_i} & I_{yz_i} & I_{zz_i} \end{bmatrix} = \begin{bmatrix} I_{xx_i}^{cm} & 0 & 0 \\ 0 & I_{yy_i}^{cm} & 0 \\ 0 & 0 & I_{zz_i}^{cm} \end{bmatrix} + m_i S(r_i)^T S(r_i) \tag{4.2}$$

where r_i denotes the position vector of the center of mass link i expressed in frame i and the skew symmetric matrix S defined as:

$$S_i = \begin{bmatrix} 0 & -r_{z,i} & r_{y,i} \\ r_{z,i} & 0 & -r_{x,i} \\ -r_{y,i} & r_{x,i} & 0 \end{bmatrix} \tag{4.3}$$

With the assumption of all links being symmetric, all the values of the products of inertia are known. They are equal to the contribution of the *Steiner* relation. Furthermore the masses and center of masses are give by the manufacturer so the first moments of inertia can also be regarded as known parameters. These known inertia elements reduce the unknown parameters in the BPS to 13.

4.3 Methodology

An specific experimental procedure is developed to determine the unknown inertial parameters of the BPS [14]. With this method a *dominant inertia* I_d is measured during experiments for each particular robot joint. This *dominant inertia* is defined as the total inertia of a manipulator link, or a group of links treated as a single link, at a certain manipulator configuration. To do this all joints are locked except for the joint from which the dominant inertia is measured. The robot manipulator can now be considered as one rigid body at that specific configuration. The dominant inertia measured at that particular joint consists of the total inertia contribution of all the links chained to the joint at that configuration. Furthermore it is important to note that the method assumes that viscous friction makes the dominant contribution to the total friction being present in the joints. The procedure of measuring the dominant inertia by experimental means is as follows.

If all joints are locked except for the specific measured joint then the single joint dynamics can be modeled as:

$$I_d\ddot{q} + \tau^f(\dot{q}) + g(q) = \tau_u \tag{4.4}$$

where $\tau^f(\dot{q})$ represents the friction present. At first the identification procedure assumes viscous friction to be dominantly present in the joints. So the following friction model is used:

$$\tau^f(\dot{q}) = f_v\dot{q} \tag{4.5}$$

As control input τ_u a normal PD control combined with gravity compensation is used:

$$\tau_u = K_p(q_d - q) + K_d(\dot{q}_d - \dot{q}) + \tilde{g}(q) \tag{4.6}$$

Where $\tilde{g}(q)$ represents the approximated gravity compensation. If it is assumed that $\tilde{g}(q) = g(q)$ then the closed loop becomes:

$$I_d\ddot{q} + f_v\dot{q} = K_p(q_d - q) + K_d(\dot{q}_d - \dot{q}) \tag{4.7}$$

By setting the desired position and desired velocity to zero the resulting equation is:

$$\ddot{q} + \frac{f_v + K_d}{I_d}\dot{q} + \frac{K_p}{I_d}q = 0 \tag{4.8}$$

If $|-K_d| = f_v$ an undamped second order system remains as:

$$\ddot{q} + \frac{K_p}{I_d}q = 0 \tag{4.9}$$

For such a system the undamped natural frequency ω_n can be calculated as follows:

$$\omega_n = \sqrt{\frac{K_p}{I_d}} \quad \Rightarrow \quad T_n = \frac{2\pi}{\sqrt{\frac{K_p}{I_d}}} \tag{4.10}$$

Equation (4.10) can be rewritten as:

$$I_d = \frac{k_p T_n^2}{4\pi^2} \tag{4.11}$$

from which the dominant inertia for the specific configuration can be solved if T_n is known from experiments.

Thus a possible procedure to solve for the dominant inertia, based on the theory above, is as follows:

- put desired angle q_d and desired velocity $\dot{q}_d$ zero as reference input for the PD control
- put K_p zero and then manually tune $-K_d$ to compensate for the viscous friction present so that the joint acts undamped. This is done by giving it an initial push by hand to overcome the static friction. Then, after releasing, the joint should maintain constant velocity.
- give K_p an positive value so that the system acts as an undamped mass-spring system.
- give an initial angle and release.
- the joint will now experience an undamped oscillation from where the undamped period T_n can be calculated by logging the angular feedback data.

Using this experiment several dominant inertias corresponding to several different robotic configurations can be determined.

To solve for the unknown inertia elements in the BPS it must be noted that a dominant inertia I_{d_i} related to released joint i corresponds to element d_{ii} from the inertia matrix D as in equation (2.3). Otherwise stated $I_{d_i} = d_{ii}$. Such a element d_{ii} is linear in some inertial elements of the BPS. So element d_{ii} can also be expressed as:

$$d_{ii}(\theta) = f_1(\theta)I_1 + f_2(\theta)I_2 + \cdots + f_m(\theta)I_m \tag{4.12}$$

Where $f_k(\theta)$ denotes a specific formula dependent of θ, the robotic configuration, and I_k denotes the corresponding specific inertia element of the BPS.

To determine the m unknown inertial elements of the BPS the element $d_{ii}(\theta)$ should be experimentally determined m times for linear independent configurations. Then the following relations appear:

$$\begin{bmatrix} d_{ii}(\theta_1) \\ d_{ii}(\theta_2) \\ \vdots \\ d_{ii}(\theta_m) \end{bmatrix} = \underbrace{\begin{bmatrix} f_1(\theta_1) & f_2(\theta_1) & \dots & f_m(\theta_1) \\ f_1(\theta_2) & f_2(\theta_2) & \dots & f_m(\theta_2) \\ \vdots & & & \vdots \\ f_1(\theta_m) & f_2(\theta_m) & \dots & f_m(\theta_m) \end{bmatrix}}_{B} \begin{bmatrix} I_1 \\ I_2 \\ \vdots \\ I_m \end{bmatrix} \tag{4.13}$$

From this the inertial parameters can be determined as they are the only unknowns. It should be noted that if the m configurations are not linearly independent then matrix B becomes singular and no solution is available.

In table 4.3 it is visible on which elements of the BPS the diagonal elements of D depend; one if it is just dependent with that factor or (θ) if there is relation that depends on the joint angles and thus on the specific manipulator configuration. The bold elements are the only unknowns though and thus the only inertial parameters that should be experimentally determined.

So, some of the inertial parameters where $d_{ii}(\theta)$ depends on are already known. If these elements are expressed as I_k then equation (4.13) can be rewritten as:

$$\begin{bmatrix} d_{ii}(\theta_1) \\ d_{ii}(\theta_2) \\ \vdots \\ d_{ii}(\theta_{k_1}) \\ \vdots \\ d_{ii}(\theta_{k_z}) \\ \vdots \\ d_{ii}(\theta_m) \end{bmatrix} = \begin{bmatrix} f_1(\theta_1) & f_2(\theta_1) & \dots & f_{k_1}(\theta_1) & \dots & f_{k_z}(\theta_1) & \dots & f_m(\theta_1) \\ f_1(\theta_2) & f_2(\theta_2) & \dots & f_{k_1}(\theta_2) & \dots & f_{k_z}(\theta_2) & \dots & f_m(\theta_2) \\ \vdots & & & & & \vdots & & \\ f_1(\theta_{k_1}) & f_2(\theta_{k_1}) & \dots & f_{k_1}(\theta_{k_1}) & \dots & f_{k_z}(\theta_{k_1}) & \dots & f_m(\theta_{k_1}) \\ \vdots & & & & & & & \vdots \\ f_1(\theta_{k_z}) & f_2(\theta_{k_z}) & \dots & f_{k_1}(\theta_{k_z}) & \dots & f_{k_z}(\theta_{k_z}) & \dots & f_m(\theta_{k_z}) \\ \vdots & & & & & \vdots & & \\ f_1(\theta_m) & f_2(\theta_m) & \dots & f_{k_1}(\theta_m) & \dots & f_{k_z}(\theta_m) & \dots & f_m(\theta_m) \end{bmatrix} \begin{bmatrix} I_1 \\ I_2 \\ \vdots \\ I_{k_1} \\ \vdots \\ I_{k_z} \\ \vdots \\ I_m \end{bmatrix} \tag{4.14}$$

Because of this known inertial parameters the number of equations to solve for the unknown inertial parameters can be reduced, and likewise the number of experiments necessary. Equation (4.14) then becomes:

$$\begin{bmatrix} d_{ii}(\theta_1) \\ d_{ii}(\theta_2) \\ \vdots \\ d_{ii}(\theta_m) \end{bmatrix} - \begin{bmatrix} f_{k_1}(\theta_1) & \dots & f_{k_z}(\theta_1) \\ f_{k_1}(\theta_2) & \dots & f_{k_z}(\theta_2) \\ \vdots & & \\ f_{k_1}(\theta_m) & \dots & f_{k_z}(\theta_m) \end{bmatrix} \begin{bmatrix} I_{k_1} \\ \vdots \\ I_{k_z} \end{bmatrix} = \underbrace{\begin{bmatrix} f_1(\theta_1) & f_2(\theta_1) & \dots & f_m(\theta_1) \\ f_1(\theta_2) & f_2(\theta_2) & \dots & f_m(\theta_2) \\ \vdots & & & \vdots \\ f_1(\theta_m) & f_2(\theta_m) & \dots & f_m(\theta_m) \end{bmatrix}}_{Bm} \begin{bmatrix} I_1 \\ I_2 \\ \vdots \\ I_m \end{bmatrix} \tag{4.15}$$

Where the columns and rows corresponding to the known inertial parameters are removed at the right side. Now the unknown inertial parameters can be solved. From table 4.1 it is obvious that the experiments should start from the last link down to the first because of the dependency on the inertial parameters.

		d_{11}	d_{22}	d_{33}	d_{44}	d_{55}	d_{66}	d_{77}
1.	$\mathbf{I_{zzR_1}}$	1						
2.	$\mathbf{I_{xxR_2}}$	(θ)						
3.	I_{xy_2}	(θ)						
4.	I_{xz_2}							
5.	I_{yz_2}							
6.	$\mathbf{I_{zzR_2}}$							
7.	mX_2							
8.	mY_{R_2}							
9.	$\mathbf{I_{xxR_3}}$	(θ)	(θ)					
10.	I_{xy_3}	(θ)	(θ)					
11.	I_{xz_3}	(θ)						
12.	I_{yz_3}	(θ)						
13.	$\mathbf{I_{zzR_3}}$	(θ)		1				
14.	mX_3	(θ)						
15.	mY_{R_3}	(θ)						
16.	$\mathbf{I_{xxR_4}}$	(θ)	(θ)	(θ)				
17.	I_{xy_4}	(θ)	(θ)	(θ)				
18.	I_{xz_4}	(θ)	(θ)					
19.	I_{yz_4}	(θ)	(θ)					
20.	$\mathbf{I_{zzR_4}}$	(θ)	(θ)		1			
21.	mX_4	(θ)	(θ)					
22.	mY_{R_4}	(θ)	(θ)					
23.	$\mathbf{I_{xxR_5}}$	(θ)	(θ)	(θ)	(θ)			
24.	I_{xy_5}	(θ)	(θ)	(θ)	(θ)			
25.	I_{xz_5}	(θ)	(θ)	(θ)				
26.	I_{yz_5}	(θ)	(θ)	(θ)				
27.	$\mathbf{I_{zzR_5}}$	(θ)	(θ)	(θ)		1		
28.	mX_5	(θ)	(θ)	(θ)				
29.	mY_{R_5}	(θ)	(θ)	(θ)				
30.	$\mathbf{I_{xxR_6}}$	(θ)	(θ)	(θ)	(θ)	(θ)		
31.	I_{xy_6}	(θ)	(θ)	(θ)	(θ)	(θ)		
32.	I_{xz_6}	(θ)	(θ)	(θ)	(θ)			
33.	I_{yz_6}	(θ)	(θ)	(θ)	(θ)			
34.	$\mathbf{I_{zzR_6}}$	(θ)	(θ)	(θ)	(θ)		1	
35.	mX_6	(θ)	(θ)	(θ)	(θ)			
36.	mY_6	(θ)	(θ)	(θ)	(θ)			
37.	$\mathbf{I_{xxR_7}}$	(θ)	(θ)	(θ)	(θ)	(θ)	(θ)	
38.	I_{xy_7}	(θ)	(θ)	(θ)	(θ)	(θ)	(θ)	
39.	I_{xz_7}	(θ)	(θ)	(θ)	(θ)	(θ)		
40.	I_{yz_7}	(θ)	(θ)	(θ)	(θ)	(θ)		
41.	$\mathbf{I_{zz_7}}$	(θ)	(θ)	(θ)	(θ)	(θ)		1
42.	mX_7	(θ)	(θ)	(θ)	(θ)	(θ)		
43.	mY_7	(θ)	(θ)	(θ)	(θ)	(θ)		

Table 4.1: Inertial dependency of diagonal elements of $D(q)$.

4.3.1 Experiment in practice

In theory (4.15) could be solved by using the exact inverse of B_n and so by using only m experiments. But, however in practice by using real experimental data this would give very inaccurate results. To avoid this problem equation 4.15 should be rewritten as:

$$\begin{bmatrix} d_{ii}(\theta_1) \\ d_{ii}(\theta_2) \\ \vdots \\ d_{ii}(\theta_w) \end{bmatrix} - \begin{bmatrix} f_{k_1}(\theta_1) & \dots & f_{k_z}(\theta_1) \\ f_{k_1}(\theta_2) & \dots & f_{k_z}(\theta_2) \\ \vdots & & \\ f_{k_1}(\theta_w) & \dots & f_{k_z}(\theta_w) \end{bmatrix} \begin{bmatrix} I_{k_1} \\ \vdots \\ I_{k_z} \end{bmatrix} = \underbrace{\begin{bmatrix} f_1(\theta_1) & f_2(\theta_1) & \dots & f_m(\theta_1) \\ f_1(\theta_2) & f_2(\theta_2) & \dots & f_m(\theta_2) \\ \vdots & & & \vdots \\ f_1(\theta_w) & f_2(\theta_w) & \dots & f_m(\theta_w) \end{bmatrix}}_{Bw} \begin{bmatrix} I_1 \\ I_2 \\ \vdots \\ I_m \end{bmatrix} \tag{4.16}$$

with $w >> m$. So w different configurations, and thus w experiments, to solve for m unknowns. Then the m unknown inertia parameters can be solved with use of the pseudo inverse defined as:

$$(B_w^T B_w)^{-1} B_w^T \tag{4.17}$$

To guarantee the existence of such a pseudo inverse it must hold that: $\det(B_w^T B_w) > 0$.

Chapter 5

Experimental results

5.1 Introduction

In Chapter 4 the theory on which the experimental determination of the inertial parameters is based is addressed. In this Chapter experimental results of using that identification method will be stated. First some practical problems encountered during experiments will be addressed in section 5.2. The results of the original experiment as suggested in Chapter 4 are given in 5.3 There will be commented on and the section will be followed by two sections, section 5.4 and 5.5, that reveal some new insights and critical aspects of the original method.

5.2 Practical problems

For a schematic representation of the experimental set-up and information about used hardware/software and corresponding abbreviations the reader is referred to appendix (B).

Amplifier gain settings

After some review it appears that the actual torque, T_{act}, that results at the joint end differs from the desired torque, T_{des}, send by the source code. To search for the cause of this difference all steps in between are considered. In the original code there appears to be an unexplainable correction gain present which is probably used before to correct for this difference. This gain is removed. Furthermore the amplifiers contain a gain, A_g, to convert their received voltage input into a corresponding ampere output to the joint actuator. The gains originally present in the amplifiers seem to be randomly chosen.

To solve the problem the value of this gain, A_g, is redetermined as follows. From the manufacturer the data as depicted in table 5.1 is known.

Table 5.1: Actuator specifications supplied by manufacturer.

Joint	$1, 2$	$3, 4$	$5, 6, 7$
Rated torque $T_r[Nm]$	5.3	2.0	0.36
Torque constant $K_T[\frac{Nm}{A}]$	0.692	0.501	0.0831

The rated torque is chosen to be the maximum that can be demanded of the specific actuator. The output range that the STG can deliver to the amplifier is minus $10[V]$ to plus $10[V]$. To utilize this full range optimally $10[V]$ received by the amplifier should correspond to an ampere output that will cause the actuator to deliver the rated torque. To ensure this the gain A_g is set as:

$$A_g = T_r \frac{1}{K_T} \frac{1}{10} \quad [\frac{A}{V}] \tag{5.1}$$

With use of the values in table 5.1 equation (5.1) gives the following gains:

Joint	$1, 2$	$3, 4$	$5, 6, 7$
$A_g[\frac{A}{V}]$	0.776	0.399	0.433

Table 5.2: Calculated amplifier gains.

To ensure that $T_{des} = T_{act}$ the source code is adapted correspondingly. After the desired torque is calculated it is transformed to the corresponding voltage output, U_{des}, and send by the STG to the amplifiers as:

$$U_{des} = T_{des} \frac{1}{A_g} \frac{1}{K_T} \frac{1}{n} \quad [V] \tag{5.2}$$

It is assumed that the manufacturer values are correct. Then it is easily verified that $T_{des} = T_{act}$ by using the AMC software[1] and directly measure the current received by the actuator. From this the output torque can easily be calculated as:

$$T_{act} = i_{measured} K_T n \quad [Nm] \tag{5.3}$$

The complete scheme as implemented in the code and present in the physical parts is visible in figure (5.1).

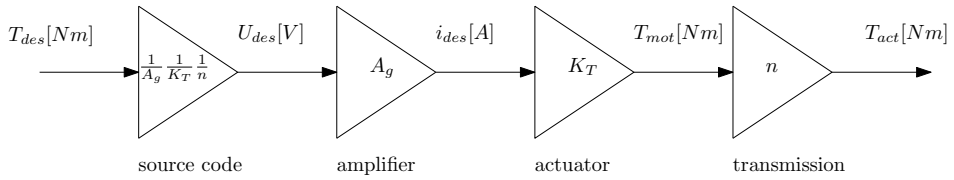

Figure 5.1: Schematic representation of gains.

Saturation settings

The output range of the STG as well as the allowable input range to the amplifiers are $\pm 10[V]$. A common error in practice is the correct handling of desired control inputs that exceed the allowable range. So here a $|U_{des}| > 10[V]$. It appears that the present algorithm in the source

[1] Advanced Motion Controller: computer software provided by the manufacturer of the amplifiers to adjust and visualize amplifier settings, measurements etcetera.

code does not suffice correctly to handle exceeded limits. Though the algorithm should nicely cap the exceeded control input to the maximum allowable input, the real torque output becomes highly unexpected when limits are exceeded.

To cope with this problem a simple *if* loop is implemented in the source code after U_{des} is calculated . The loop just acts as a saturation before the limits are exceeded. An important thing to notice however, is that for the saturation limits not the real limits of $\pm 10[V]$ are used. The limits are chosen more moderate. This has to be done because of an offset being present in the amplifiers. If the source code would exactly cap at the limits of $\pm 10[V]$, so the STG can handle, then the STG would nicely sends $\pm 10[V]$ to the amplifier. The receiving amplifier can still not handle this properly because of the offset being present that is added on to the receiving STG signal. To be on the safe side and prevent exceeding the limits of the amplifier, the source code loop acts as a saturation with limits of $\pm 9.7[V]$.

Saturated velocity

Another problem encountered during experiments is the joint velocity saturating before the maximum joint velocity, as supplied by the manufacturer, is reached. Originally the experimental set-up was working with a power supply delivering $24[V]$. It appears that the following physical balances limit the velocity before the maximum joint velocity is reached in case of using $24[V]$ as power supply:

$$U_{pow} = K_T \dot{\theta}_m + iR + L\frac{d}{dt}i \tag{5.4}$$

The last term can be neglected because of $L << R$. Furthermore the current i is related to the mechanical balance as:

$$K_T i = \tau \tag{5.5}$$

So a certain required torque output τ requires a corresponding i related as in (5.5). Using this required i (5.4) still has to be in balance so the velocity $\dot{\theta}$ will adapt accordingly to comply to this. In case of U_{pow} being $24[V]$ this balances will result in $\dot{\theta}$ saturating before reaching the maximum joint velocity as supplied by the manufacturer. To avoid this saturation problem the simple solution is to use $48[V]$ as power supply.

5.3 Results original procedure

To verify that the method as suggested in Chapter 4 indeed works, the experiment is first applied for only one configuration, namely the robot in upright position, and only on joint 1. So the robotic manipulator is temporarily regarded as an 1 d.of. system. Then the experiment determines the inertia corresponding to that specific upright position for movement of joint 1, I_{exp}. Next this measured inertia can be used in trajectory control of joint 1 with the robot still in fully upright position as:

$$\tau_u = I_{exp}\, \ddot{q}_d + K_p(q_d - q) + K_d(\dot{q}_d - \dot{q}) \tag{5.6}$$

Adding this feed-forward term should clearly improve the control performance if I_{exp} is correct. Like this the identification methodology can be easily verified by doing so. It must be noted

that the encountered phenomena as described below hold for all joints as is experienced during experiments.

The first step as described before in Chapter 4 is to manually tune $-K_d$ in the PD-control to compensate for the viscous friction present in the system. After slowly increasing $-K_d$ (making it more negative) the following phenomena appear to be the case:

- $|-K_d| < 12$ results in a damped motion after releasing the joint with an initial velocity.
- $|-K_d| = 12$ is the first value that can keep the velocity going but only if the initial velocity when released is close to the maximum velocity of the joint. If that is the case, then the velocity will remain the maximum joint velocity. Else, in the case of a lower initial velocity, the system still acts damped and the velocity settles at zero.

This last phenomenon is clearly not as expected by the theory. According to the model as in (4.8) there are three possible situations. For clearness the model is recapitulated as:

$$\ddot{q} + \frac{f_v + K_d}{I_d}\dot{q} + \frac{K_p}{I_d}q = 0 \tag{5.7}$$

Then the three possible situations are:

1. $|-K_d| < f_v$, in which the system is undercompensated and *all* initial velocities will go to zero after releasing.
2. $|-K_d| = f_v$, in this case the viscous friction is exactly compensated and the system will perfectly act as an undamped system. If that is the case then *all* initial velocities should maintain constant after releasing.
3. $|-K_d| > f_v$, in which the system is overcompensated and *all* initial velocities will keep accelerating till the maximum joint velocity is reached.

Clearly none of this three situations correspond to the encountered phenomenon; some initial velocities that completely damp to zero *and* initial velocities that result in maintaining maximum joint velocity.

Hypothesis

The original procedure as suggested is fully based on the assumption that viscous friction dominates the total friction being present in the joints. However, the first results do not seem to support this assumption as clearly none of the three possible situations above fits the phenomenon. A plausible explanation is that Coulomb friction seems to be significantly present and modeling only viscous friction compensation is insufficient.

If this is indeed the case then the situation present is probably as in figure 5.2. So in the case of Coulomb friction being significantly present it is never possible to align the compensated friction with the real friction if there is only compensated for viscous friction. Then there are two possible situations that can occur. The compensated friction has no intersection point with the real friction and is thus always smaller. This results in all initial velocities damp to zero. Another possibility is that the compensated friction intersects with the real friction. This situation is visualized in the figure by intersection point a. If this kind of situation is present then the encountered phenomena can be explained as follows;

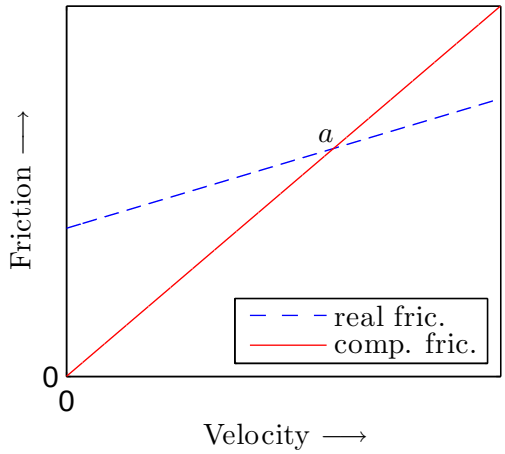

Figure 5.2: Expected relation between real friction being present and compensated friction.

- if the initial velocity after releasing is to the left side of intersection point a then the system is undercompensated and the velocity will damp.
- if the initial velocity after releasing is to the right side of intersection point a then the system is overcompensated and will keep on acceleration till the maximum joint velocity is reached.

Friction identification

To prove the stated hypothesis, i.e. Coulomb friction is significantly present and therefore an intersection point between the compensated and real friction is possible which causes the phenomenon, a rough friction identification is done. The friction identification procedure used is as follows; as a reference signal for the velocity a trapezoidal input V_{des} is used, see figure 5.3. The corresponding position reference signal is calculated. These two reference signals are used for normal PD control.
On the horizontal parts of the trapezoidal the velocity is constant and thus the acceleration is zero. For the parts where the acceleration is zero the following change of the original single joint model

$$I\ddot{q} + \tau^f(\dot{q}) + g(q) = \tau_u \tag{5.8}$$

in to

$$\tau^f(\dot{q}) + g(q) = \tau_u \tag{5.9}$$

holds. For the robot in upright position $g(q)$ has no effect on following this desired trapezoidal velocity pattern for joint 1, 3 and 5. For joint 2 and 4 however, the robot is brought in horizontal position to cancel gravitational effects. Then the gravitational term can be canceled and (5.9) becomes:

$$\tau^f(\dot{q}) = \tau_u \tag{5.10}$$

From (5.10) it is clear that the control input force τ_u is equal to the experienced friction force τ^f. For one data point the mean of the input control torque, figure 5.4, on the horizontal parts

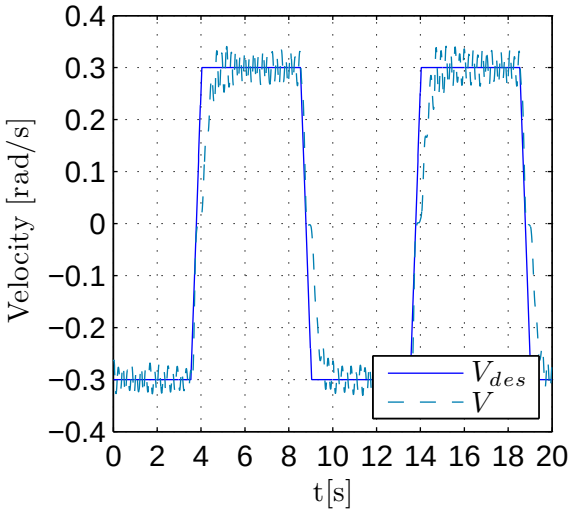

Figure 5.3: Desired velocity with measured velocity.

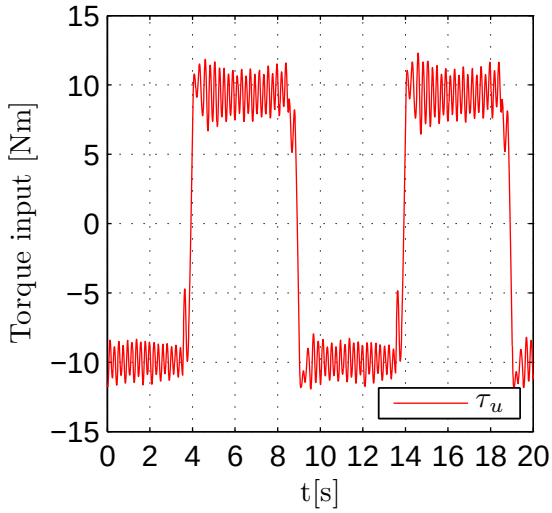

Figure 5.4: Torque input τ_u.

of the trapezoidal velocity pattern is taken. This force value represents the friction force for the corresponding velocity as given by the trapezoidal input. With use of this method several data points for different velocities are gathered to do a friction identification. The friction identification consists of a least-square fit through the gathered data points. The model used for this fit is based on Coulomb and viscous friction like described before in equation (2.21):

$$\tau_{vc}^{f}(t) = f_v\dot{q} + f_c\text{sign}(\dot{q}) \tag{5.11}$$

Here only the result of this friction identification for joint 1 is discussed. All other joint identifications and corresponding identified values f_v and f_c are given in appendix (C).

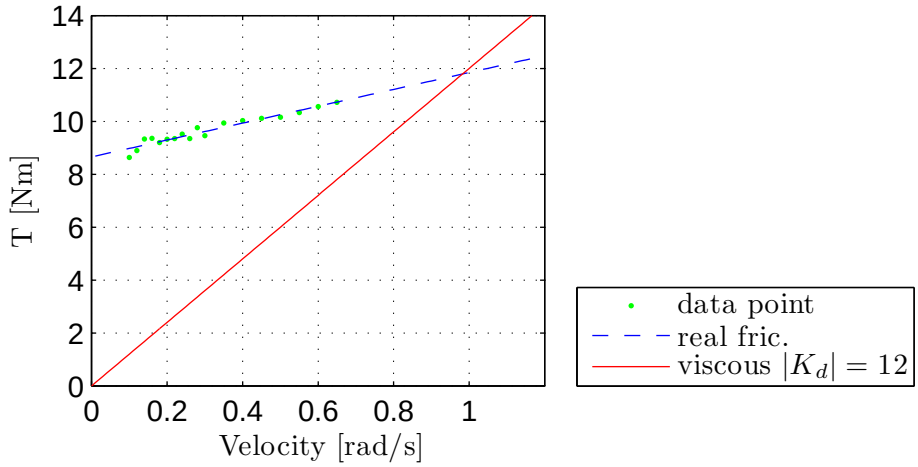

Figure 5.5: Relation between identified real friction being present and compensated friction.

The identification result (dashed line) for joint 1 is visible in figure 5.5. To prove that the friction as identified is indeed correct it is added to normal PD control to compensate for the friction. For

the same PD control values and the same reference signal the error reduction because of added friction compensation is visible in figure 5.6

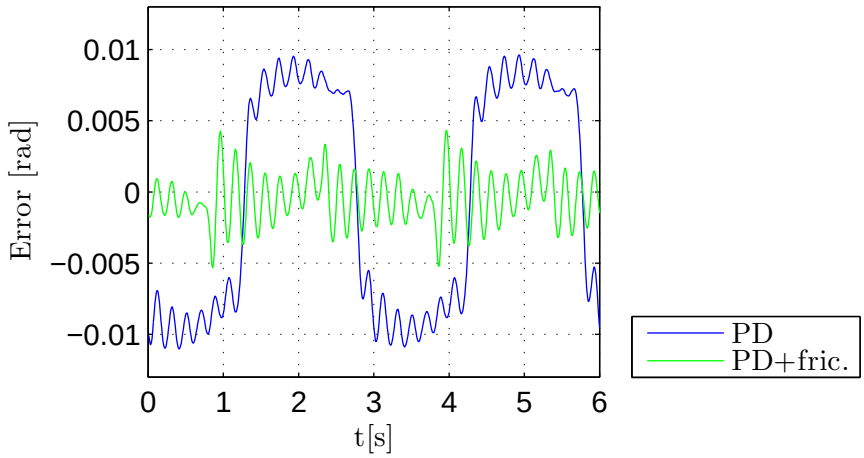

Figure 5.6: Error reduction with use of identified friction compensation.

With a considerable error reduction being obviously present it is proven that the friction compensation as added to the PD control is of good quality. The friction compensation is based on the experimentally identified friction as visible in figure 5.5. Thus the experimentally procedure used gives an identified friction model of good quality. Then, looking at the identified friction model in figure 5.5 it is clear that the Coulomb friction adds a significant part to the total friction. The hypothesis stated earlier, that a Coulomb part being significantly present is the cause to the phenomenon, is correct because the behaviour matches with figure 5.5. The compensation as used in the original procedure is also visible in the figure for $K_d = -12$. This is the first value that can keep the velocity constant after releasing, though only when released at almost maximum joint velocity ($q_{max} = 1.2[rad/s]$). This can be explained with use of the graph. $K_d = -12$ is the first friction compensation that has a slope steep enough to ensure that the intersection point between the compensated friction and the real friction is within the possible velocity range. Indeed it is correct that the velocity always acts undercompensated, so damped, if it is to the left side of this intersection point and indeed it can only keep constant velocity at maximum velocity because there the systems friction is overcompensated.

This result affects the original identification method as described in Chapter 4. To be able to get an undamped system, and consequently being able to measure the undamped eigenfrequency, the original model for the procedure as suggested in equation (4.4) has to be expanded with Coulomb friction. Thus the new model becomes:

$$I_d\ddot{q} + \tau_{vc}^f(\dot{q}) + g(q) = \tau_u \quad \text{with} \quad \tau_{vc}^f(\dot{q}) = f_v\dot{q} + f_c\text{sign}(\dot{q}) \tag{5.12}$$

5.4 Results using identified friction

Now the friction present in the system is experimentally identified this result is used to make the joint act as an undamped system using the following control:

$$\tau_u = \tilde{\tau}^f_{vc} \quad \text{with} \quad \tilde{\tau}^f_{vc} = \tilde{f}_v\dot{q} + \tilde{f}_c\text{sign}(\dot{q}) \tag{5.13}$$

Here $\tilde{\tau}^f_{vc}$ represents the identified friction, with the identified values $\tilde{f}_v$ and $\tilde{f}_c$ that follow from the least-square fit through the data.

To verify that the system indeed acts undamped, joint 1 is released for different initial velocities initiated with use of trapezoidal control as used before to do friction identification. If the velocity is on the constant part of the trapezoidal velocity trajectory then the controller used to track the trapezoidal reference signal is stopped by switching to the controller of equation (5.13). For an undamped system the velocity should remain nicely constant. The result is visible in figure (5.7). It is clearly visible that the velocity does not remain constant as expected. The figure gives not enough information to draw real conclusions about the systems behaviour.

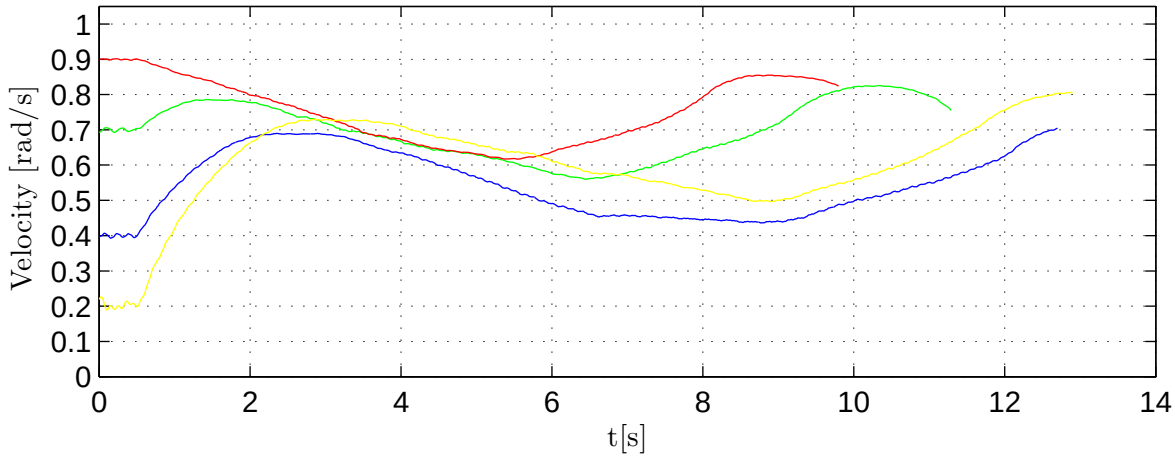

Figure 5.7: Velocity behaviour using identified friction compensation.

Because it is obvious that practical results always differ from the ideal case, and on first sight there does not seem to be a better alternative then the friction identification done before, that is to guarantee an undamped system, the identification procedure is continued to find the inertia value for joint 1 in upright position. Therefore K_p is added to equation (5.13). The new control input thus becomes:

$$\tau_u = -K_p q + \tilde{\tau}^f_{vc} \quad \text{with} \quad \tilde{\tau}^f_{vc} = \tilde{f}_v\dot{q} + \tilde{f}_c\text{sign}(\dot{q}) \tag{5.14}$$

If the systeem is indeed undamped then a constant oscillation wil remain with an amplitude equal to an initial angle offset. The result is visible in figure(5.8). Although the system indeed ends up in a constant undamped oscillation it is remarkable that the amplitude for different initial offsets ends up to be the same. So the system behaves as if there is a stable limit cycle present. In the next section this will be confirmed.

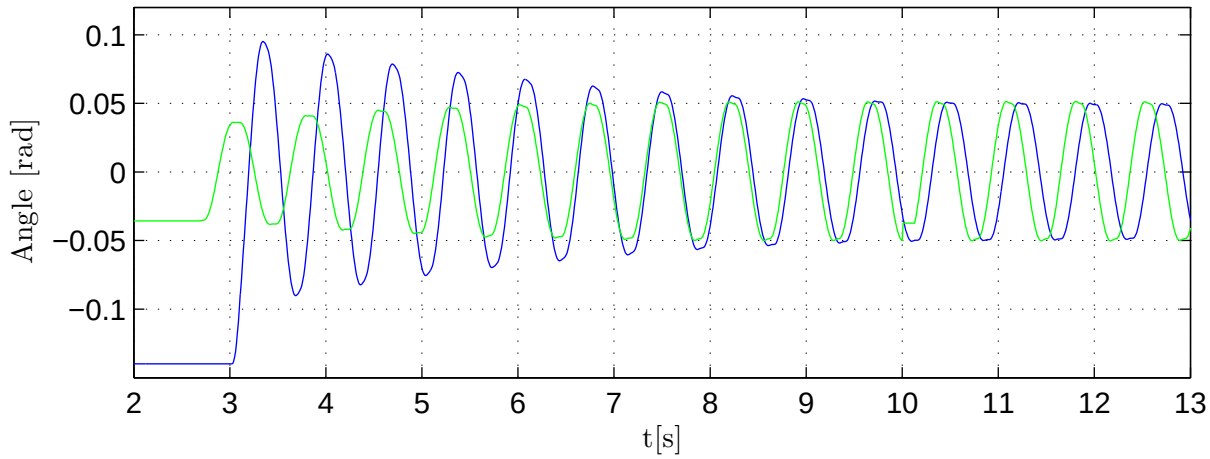

Figure 5.8: Angular motion.

To be conclusive that the improved inertia identification method, i.e. with identified friction instead of manually tuned friction compensation, does not give satisfactory results the inertia is calculated for different K_p. In case of an undamped system the period should change accordingly to K_p so that equation (4.11) always gives the same inertia. In figure (5.9) the calculated inertia is plotted against the K_p used. Each experiment with a different value for K_p is performed twice to verify its repeatability. A horizontal line is expected but the result appears to be that a different K_p does affect the calculated inertia outcome. It is clear that this experimental result is not satisfactory and that the applied improved identification procedure is not suitable.

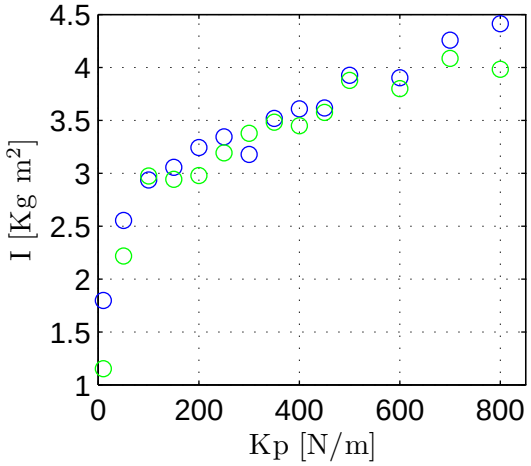

Figure 5.9: Influence of K_p.

5.5 Friction influence in practice

In the previous section it is shown that, despite the usage of an experimentally identified friction model, the friction compensation still does not result in satisfying a fully undamped system. Even if the friction is identified by experimental means it is never perfectly identical to the real friction. The original inertia identification method as described in Chapter 4 is based on the assumption that this difference between compensated and real friction does not effect the systems behaviour significantly. It expects the system to approach undamped behaviour good enough to gain useful experimental data. However in practice this seems not to be the case. The imperfection in friction compensation results in a specific corresponding system behaviour.

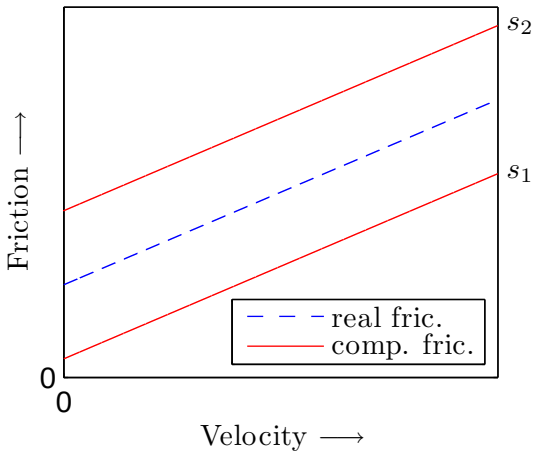

Figure 5.10: Friction compensation v.s. real friction present; situation s_1 and s_2.

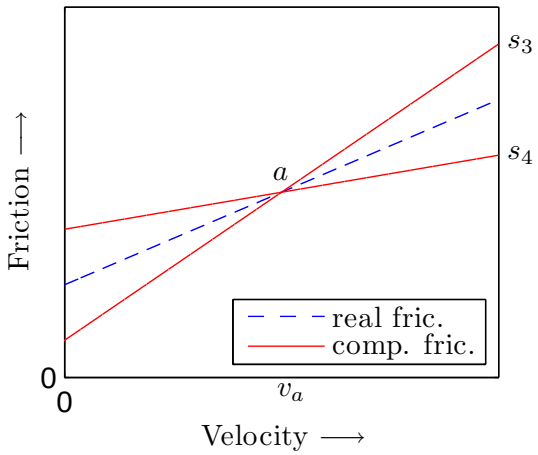

Figure 5.11: Friction compensation v.s. real friction present; situation s_3 and s_4.

Because the emphasis of this report is not on friction identification but on the usage of the identification method of Chapter 4 for identification of system parameters, our analysis of the influence of real friction versus compensated friction is restricted to the widely excepted and used friction model that consists of a viscous and Coulomb part as in 2.21. For a much more thorough research to the effects of imperfect friction compensation in mechanical systems the reader is referred to [20].

If the friction models are only based on viscous and Coulomb then there are four different situations of imperfect friction compensation. The four situations are depicted in figures 5.10 and 5.11. Situation s_1 and s_2 are straightforward in their behaviour. In the case of situation s_1 the system is always undercompensated for the real friction and therefore the initial velocity will always, regardless of its value, damp to zero. In the case of situation s_2 the system is always overcompensated for the real friction and therefore the initial velocity, again regardless of its value, will always keep increasing till the maximum possible joint velocity is reached.

More interesting are situation s_3 and s_4. They differ from the other two in having an intersection point (a) with the real system friction. Situation s_3 is almost similar as experienced with the original friction compensation; only now inclusive some small Coulomb part. The behaviour for this two situations is expected to be as follows; in the case of situation s_3 the system will act damped if the intial velocity is in the range to the left of intersection point a ($v < v_a$). Otherwise, if the initial velocity is in the right range of intersection point a ($v > v_a$), the system will be overcompensated and velocity will increase till the maximum joint velocity is reached. In the

case of situation s_4 the system will always settle at the velocity that corresponds to the intersection point a, v_a. If the initial velocity is in the left range of intersection point a then the system is overcompensated and the velocity will increase. This increasing stops if the velocity crosses the velocity that corresponds to the intersection point. After the intersection point the system is undercompensated and the velocity will experience damping. So the velocity will decrease again till the intersection point. If the initial velocity is in the right range of the intersection point the opposite happens, first decreasing velocity and then increasing velocity till it is settled in the velocity again that corresponds to the intersection point. In the previous section a limit cycle was encountered. With use of simulations with a Matlab Simulink model this observed behaviour is confirmed when a stiffness K_p is added; for the case of situation s_4 there appears to be a stable limit cycle. Physically this can be explained as follows; for low velocities the system gains energy because of the control overcompensation and at higher velocities the system is subjected to energy loss because of friction undercompensation, so damping.
The described behaviour above, the settled end velocity for different initial velocities, for the different situations can be graphically represented as visible in figures (5.12) and (5.13).

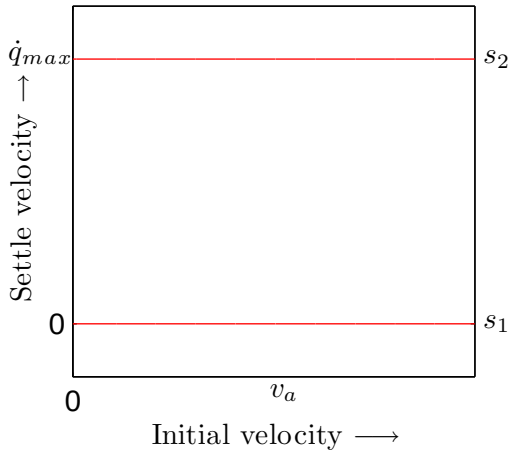

Figure 5.12: Settled velocity versus initial velocity; situation s_1 and s_2.

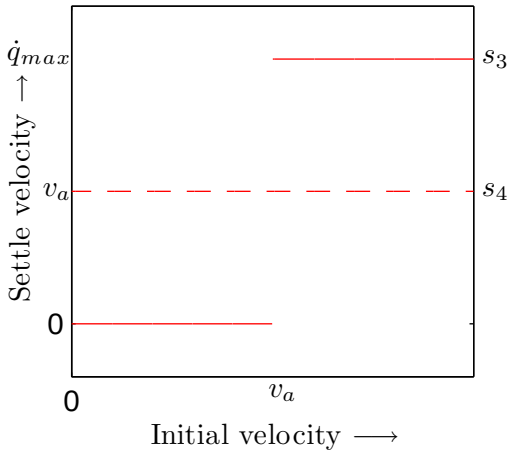

Figure 5.13: Settled velocity versus initial velocity; situation s_3 and s_4.

That the behaviour of the system for situation s_3 and s_4 is indeed as described before is first verified using experiments. Based on the identified friction for joint 1 as visible in figure (5.5) two different friction compensations are used that are sure to guarantee situation s_3 and s_4. The experimental results for situation s_3 and s_4 are visible in figure (5.14) and figure (5.15) respectively. They confirm the expected behaviour. In figure (5.14) velocity v_a, and thus the corresponding intersection point a is somewhere between $0.4[rad/s]$ and $0.7[rad/s]$. In figure (5.15) the settled velocity v_a is approximately $0.5[rad/s]$.

All the system behaviour encountered during experiments for system identification, based on the theory of Chapter 4, fit one of the described behaviours above corresponding to one of the four different situations. This shows that even a slight difference between compensated and real friction gives a system behaviour that can not be regarded as fully undamped.

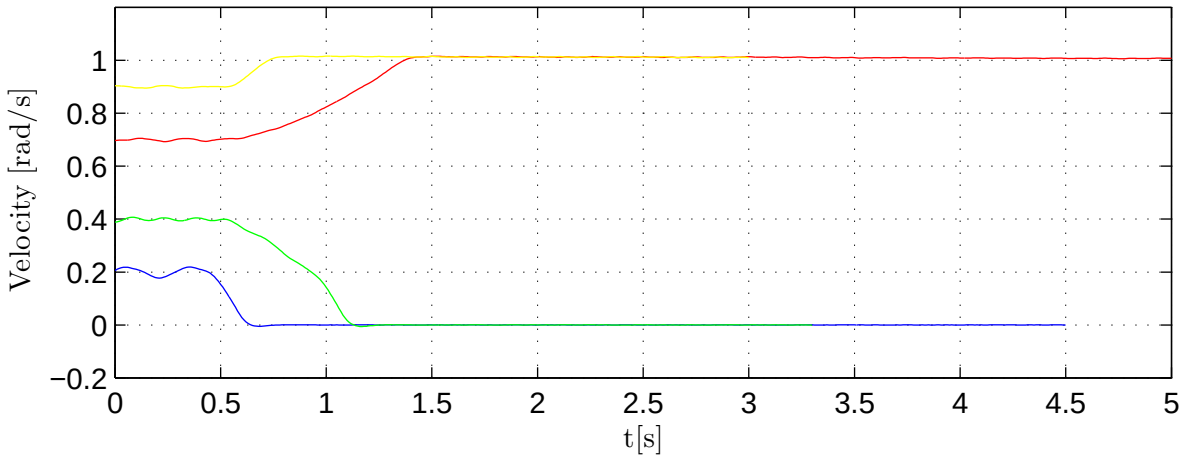

Figure 5.14: Velocity behaviour for situation s_3.

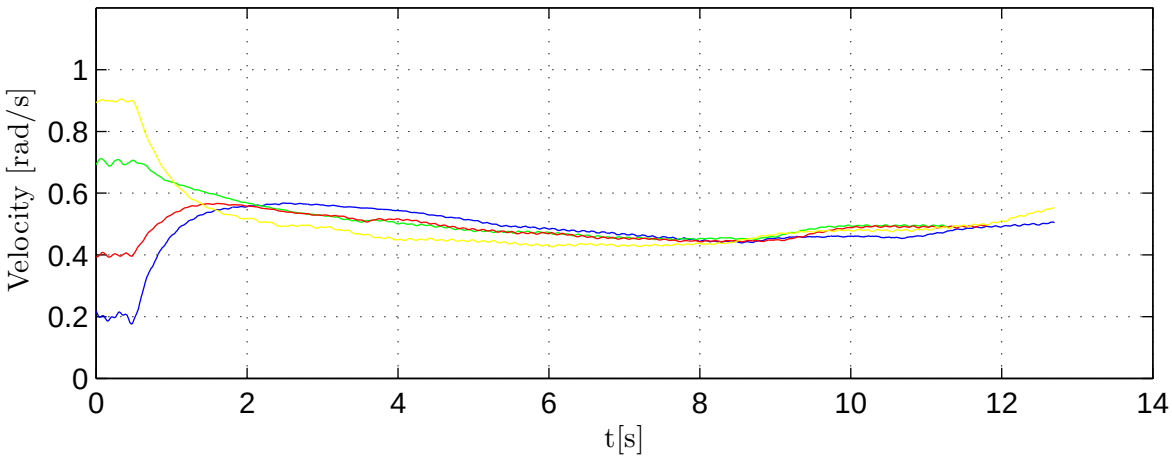

Figure 5.15: Velocity behaviour for situation s_4.

Chapter 6

Conclusions and Recommendations

6.1 Introduction

The research objective is recapitulated as; describe the complete dynamics of the Mitsubishi PA-10 robotic manipulator and identify all unknown system parameters, used in the obtained dynamic model, by experimental means. The applied identification method, as proposed by SIMtech, is explained in Chapter 4. Experimental results using the identification method are shown in Chapter 5. These results show that the identification method in practical applications does not give the results that correspond to the theoretical foundations. In the next paragraph research results and issues regarding the identification method will be discussed followed by recommendations for future research.

6.2 Contribution

- The complete symbolically dynamical model is derived for the Mitshubishi PA-10 manipulator. This model is reduced in complexity to make it suitable to use in identification procedures. This reduction is done in a well-structured way that gives the base parameter set of 43 inertia parameters. Furthermore some other assumptions led to further reduction of the mathematical model (13 unknowns left) to diminish the burden of experimental inertia identification.
- It is shown that the original identification procedure, based on the assumption of real friction being dominated by viscous friction, is not suitable for the PA-10. Using friction identification by experimental means it is proven that Coulomb friction is significantly present in the joints.
- Relating the previous observation that only viscous friction compensation does not suffice, the real friction present is experimentally identified for all joints. It is shown that the gained identified friction model gives substantial improvement if used as friction compensation in trajectory control.
- Furthermore it is shown that even by using an experimentally identified friction model for friction compensation, the proposed identification method is too sensitive to imperfections in correct friction compensation. Four different situations of imperfect friction compensation are considered and their expected behaviour is confirmed by experimental means.

The general conclusion of the research is that the identification method based on finding an undamped system is very nice in theory but not suitable for practical applications. The reason for this is that in practice researchers can never succeed in achieving perfect compensation for the real friction being present. So this unavoidable imperfection will always result in joint behaviour not equal to a nicely undamped system. The sensitivity of the identification method for this imperfection is that large that identified results are worthless. Therefore the identification method should be regarded impractical and it can not be used to identify system parameters as supported by erroneous identification results.

6.3 Recommendations

The main obstacle present for succeeding in the implementation of model-based control is identifying the full dynamics of the robotic manipulator. It is shown that the originally proposed identification method is not suitable in practice to achieve this. If the general objective of SIMtech is kept in mind, implementing force control using model-based control, then the following recommendations for future research are done:

- Worldwide there has been a lot of research on the topic of system parameter identification. In this report no attention is spent to investigating alternatives. In Chapter 3 some of the common identification methods are mentioned though. Based on experimental results shown in literature, making use of an identification method using derived velocity information in combination with external torque/force information measured on a bedplate supporting the robotic manipulator seems a promising alternative. Investing time in finding a suitable alternative is recommended. For most identification methods the dynamic model, including the derivation of the base parameter set and other simplifications, as described in Chapter 2 is still suitable to use.

- The influence of friction compensation has been topic of many researches. Some researches focus specifically on the effects of under- and overcompensation on system behaviour [20]. Maybe there are possibilities to use all this available knowledge to adapt the original identification procedure and making it less sensitive for the effects of frictions.

- Another possibility to avoid the difficulty of system identification is the use of adaptive robot control. By using an adaptive model system parameters will converge during control experiments and no system identification in advance of model-based control is required [21].

References

[1] John J. Craig, "Introduction to Robotics: mechanics and control", 2nd edition, Addison-Wesley, 1989

[2] L. Sciavicco and B. Siciliano, "Modeling and control of robot manipulators", 2nd edition, Springer,

[3] Mark. W. Spong, Seth Hutchinson and M. Vidyasagar, "Robot Modeling and Control", Wiley, 2006

[4] P.I. Corke, "A Robotics Toolbox for Matlab", IEEE Robotics and Automation Magazine, vol.3, no.1, pp.24-32, 1996

[5] Mitsubishi Heavy Industries LTD, "PA-10 portable general purpose intelligent arm, operating manual", 9100025 rev1.

[6] Jan Swevers, Walter Verdonck and Joris de Schutter, "Dynamic Model Identification for Industrial Robots", IEEE Control Systems Magazine, oct., pp.58-71, 2007

[7] G. Antonelli, F. Caccavale and P. Chiacchio, "A systematic procedure for the identification of dynamic parameters of robot manipulators", Robotica, vol. 17, pp.427-435, Cambridge University Press, 1999

[8] Fariborz Behi and Delbert Tesar, "Parametric Identification for Industrial Manipulators Using Experimental Modal analysis", IEEE Transactions on Robotics and Automation, vol. 7, no.5, pp.642-652, October 1991

[9] P.O. Vandanjon, M. Gautier and P. Desbats, "Identification of Robots Inertial Parameters by Means of Spectrum Analysis", IEEE International Conference on Robotics and Automation, pp. 3033-3038, 1995

[10] M. Gautier, "A Comparison of Filtered Models for Dynamic Identification of Robots", Proceedings of the 35th Conference on Decision and Control, pp.875-880,Kobe, Japan, 1996

[11] M. Gautier, "Dynamic Identification of Robots with Power Model", Proceedings of the 1997 IEEE International on Robotics and Automation, pp.1922-1927, Albuquerque, New Mexico, April 1997

[12] J. Swevers et. all, "Experimental identification of robot dynamics for control", Proceedings of the 2000 IEEE International Conference on Robotics and Automation, pp.241-246, San Francisco, CA, April 2000

[13] Peter I. Corke and Brian Armstrong-Helouvry, "A Search for Consensus Among Model Parameters Reported for the PUMA 560 Robot", IEEE, pp.1608-1613, 1994

[14] Rodrigo S. Jamisola, JR., "Full Dynamics Identification and Control of PUMA 560 and Mitsubishi PA-10 robots", thesis produced at National University Singapore, ME department, 2001

[15] M. Gautier and W. Khalil, "A direct determination of minimum inertial parameters of robots", IEEE, 1988

[16] M. Gautier and W. Khalil, "Direct Calculation of Minimum Set of Inertial Parameters of Serial Robots", IEEE Transactions on Robotics and Automation, vol. 6, no.3, pp.368-373, June 1990

[17] W. Khalil and F. Bennis, "Comments on 'Direct Calculation of Minimum Set of Inertial Parameters of Serial Robots'", IEEE Transactions on Robotics and Automation, vol. 10, no.1, pp.78-79, February 1994

[18] Nikolas A. Bompos et all., "Modeling full identification and Control of the Mitsubishi PA-10 Robot Arm", Control Systems Lab, School of Mechanical Eng. National Technical University of Athens, publication date unknown

[19] Christopher W. Kennedy et all., "Modeling and Control of the Mitsubishi PA-10 Robot Arm Harmonic Drive System", IEEE Transactions on Mechatronics, vol. 10, no.3, pp.263-274, June 2005

[20] D. Putra, H. Nijmeijer and N. van de Wouw, "Analysis of undercompensation and overcompensation of friction in 1DOF mechanical systems", Automatica, no.43, pp.1387-1394, Elsevier, June 2007

[21] H. Berghuis, H. Roebbers and H. Nijmeijer, "Experimental Comparison of Parameter Estimation Methods in Adaptive Robot Control", Automatica, vol. 31, no.9, pp.1275-1285, Elsevier, 1995

Appendix A

Equations Base Parameter Set

Link 7:

$$\left.\begin{array}{lcllll} I_{xxR_7} & = & I_{xx_7} & -I_{yy_7} & & \\ I_{xxR_6} & = & I_{xx_6} & +I_{yy_7} & 2d_7mZ_7 & +d_7^2m_7 \\ I_{zzR_6} & = & I_{zz_6} & +I_{yy_7} & 2d_7mZ_7 & +d_7^2m_7 \\ mY_{R_6} & = & mY_6 & -mZ_7 & -d_7m_7 & \\ m_{R_6} & = & m_6 & +m_7 & & \end{array}\right\} \tag{A.1}$$

So the base parameters of link 7 are: $I_{xxR_7},\ I_{xy_7},\ I_{xz_7},\ I_{yz_7},\ I_{zz_7},\ mX_7,\ mY_7$.

Link 6:

$$\left.\begin{array}{lcll} I_{xxR_6} & = & I_{xxR_6} & -I_{yy_6} \\ I_{xxR_5} & = & I_{xx_5} & +I_{yy_6} \\ I_{zzR_5} & = & I_{zz_5} & +I_{yy_6} \\ mY_{R_5} & = & mY_5 & +mZ_6 \\ m_{R_5} & = & m_5 & +m_6 \end{array}\right\} \tag{A.2}$$

So the base parameters of link 6 are: $I_{xxR_6},\ I_{xy_6},\ I_{xz_6},\ I_{yz_6},\ I_{zzR_6},\ mX_6,\ mY_{R_6}$.

Link 5:

$$\left.\begin{array}{lcllll} I_{xxR_5} & = & I_{xxR_5} & -I_{yy_5} & = I_{xx_5} + I_{yy_6} - I_{yy_5} & \\ I_{xxR_4} & = & I_{xx_4} & +I_{yy_5} & +2d_5mZ_5 & +d_5^2m_{R_5} \\ I_{zzR_4} & = & I_{zz_4} & +I_{yy_5} & +2d_5mZ_5 & +d_5^2m_{R_5} \\ mY_{R_4} & = & mY_4 & -mZ_5 & -d_5m_{R_5} & \\ m_{R_4} & = & m_4 & +m_{R_5} & = m_4 + m_5 + m_6 & \end{array}\right\} \tag{A.3}$$

So the base parameters of link 5 are: $I_{xxR_5},\ I_{xy_5},\ I_{xz_5},\ I_{yz_5},\ I_{zzR_5},\ mX_5,\ mY_{R_5}$.

Link 4:

$$\left.\begin{array}{lcll} I_{xxR_4} & = & I_{xxR_4} \; -I_{yy_4} & = I_{xx_4} + I_{yy_5} + 2d_5 mZ_5 + d_5^2 m_{R_5} - I_{yy_4} \\ I_{xxR_3} & = & I_{xx_3} \; +I_{yy_4} & \\ I_{zzR_3} & = & I_{zz_3} \; +I_{yy_4} & \\ mY_{R_3} & = & mY_3 \; +mZ_4 & \\ m_{R_3} & = & m_3 \; +m_{R_4} & = m_3 + m_4 + m_5 + m_6 \end{array}\right\} \quad (A.4)$$

So the base parameters of link 4 are: $I_{xxR_4},\ I_{xy_4},\ I_{xz_4},\ I_{yz_4},\ I_{zzR_4},\ mX_4,\ mY_{R_4}$.

Link 3:

$$\left.\begin{array}{lcllll} I_{xxR_3} & = & I_{xxR_3} & -I_{yy_3} & = I_{xx_3} + I_{yy_4} - I_{yy_3} & \\ I_{xxR_2} & = & I_{xx_2} & +I_{yy_3} & +2d_3 mZ_3 & +d_3^2 m_{R_3} \\ I_{zzR_2} & = & I_{zz_2} & +I_{yy_3} & +2d_3 mZ_3 & +d_3^2 m_{R_3} \\ mY_{R_2} & = & mY_2 & -mZ_3 & -d_3 m_{R_3} & \end{array}\right\} \quad (A.5)$$

So the base parameters of link 3 are: $I_{xxR_3},\ I_{xy_3},\ I_{xz_3},\ I_{yz_3},\ I_{zzR_3},\ mX_3,\ mY_{R_3}$.

Link 2:

$$\left.\begin{array}{lcll} I_{xxR_2} & = & I_{xxR_2} \; -I_{yy_2} & = I_{xx_2} + I_{yy_3} + 2d_3 mZ_3 + d_3^2 m_{R_3} - I_{yy_2} \\ I_{zzR_1} & = & I_{zz_1} \; +I_{yy_2} & \end{array}\right\} \quad (A.6)$$

So the base parameters of link 2 are: $I_{xxR_2},\ I_{xy_2},\ I_{xz_2},\ I_{yz_2},\ I_{zzR_2},\ mX_2,\ mY_{R_2}$.

Link 1:
Because of *Theorem 3* the minimum parameter of link 1 is I_{zzR_1}.

So this regrouping of inertial parameters reduces the number of inertial parameters from 60 to 43. (22 if you would not take the diagonal terms of the inertia matrices, so the products of inertia (for example I_{xz_i} etc.) in to account).
Theorem 7: minimum base parameters set $\leq n * 7 - 4 = 45$. Here 43 because: -2 because axis z_1 is equal to the gravity vector.

Appendix B

Experimental setup

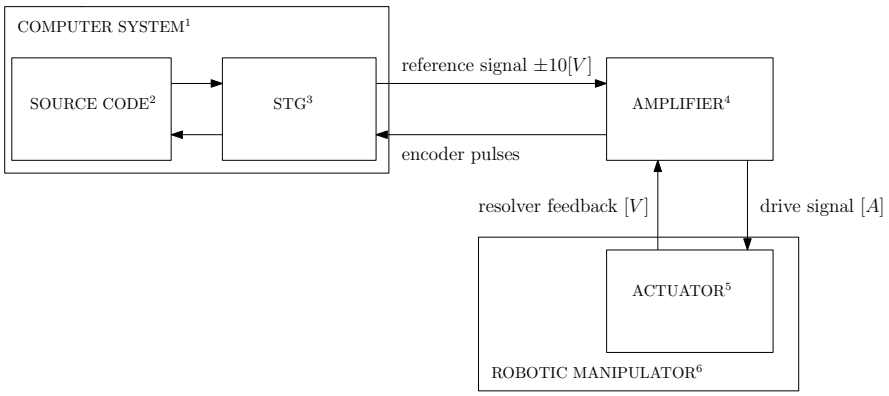

Figure B.1: Experimental set-up.

A schematic representation of the experimental set-up is visible in figure B.1. Technical specifications of the computer system used for control and measurements and some other useful technical data can be found below.

1. Computer system:	Microsoft Windows XP in combination with Realtime Extension for Windows (RTX) sample rate: $1000[Khz]$
2. Source code:	c-code build with Microsoft Visual Studio 6.0, GUI build with Microsoft Visual Basic 6.0
3. Server To Go (STG):	model 2-8 axis ISA servo i/o card
4. Amplifier:	Advanced Motion Controller (AMC), model Digiflex; digital servo drive CDD005BB
5. Actuator:	See technical specifications reference [5], chapter 5 pg.13-14
6. Robotic manipulator:	7 d.o.f. robotic manipulator, see figures (1.1), (2.1). See technical specifications reference [5]

Appendix C

Friction identifications

[1]

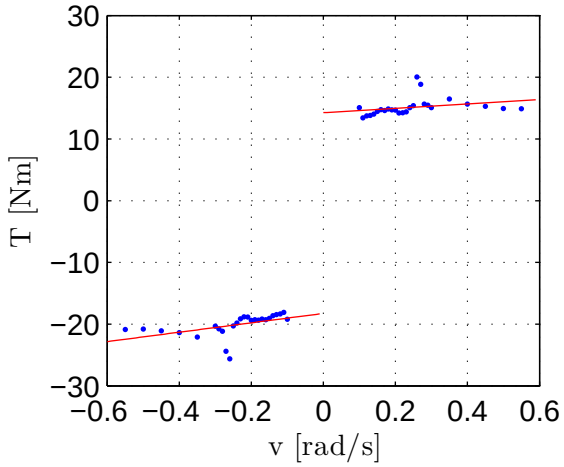

Figure C.1: Friction identification joint 2.

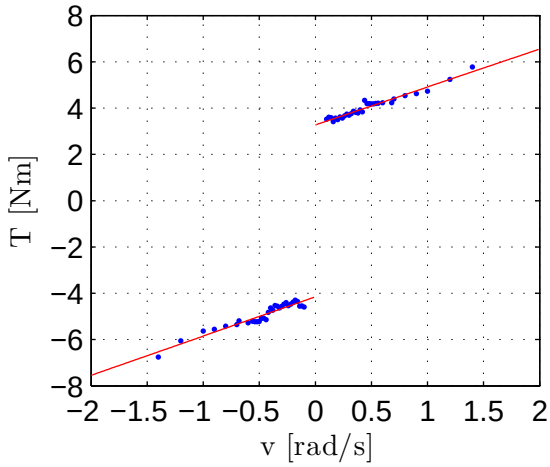

Figure C.2: Friction identification joint 3.

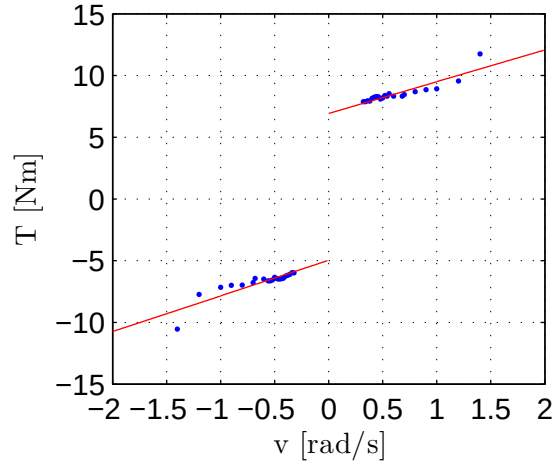

Figure C.3: Friction identification joint 4.

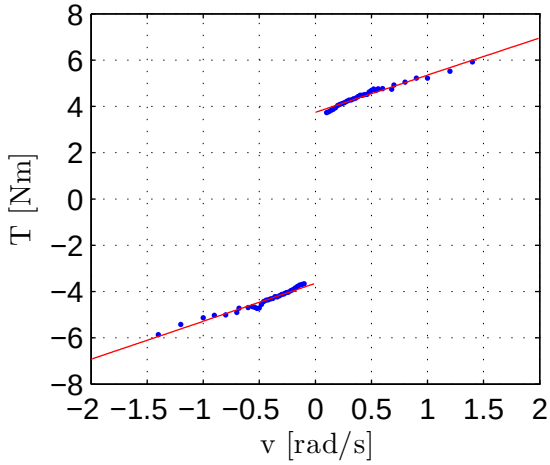

Figure C.4: Friction identification joint 5.

[1] During the research period joint 6 was broke so no results of joint 6 are available.

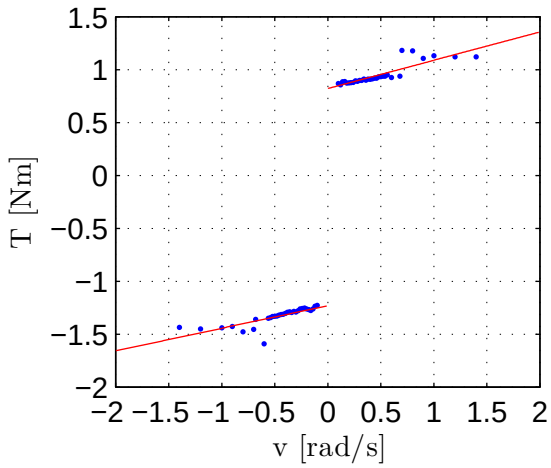

Figure C.5: Friction identification joint 7.

The friction compensations are fitted with the formula of equation (2.21) as:

$$\tau_{vc}^{f}(t) = f_{v_n}\dot{q} + f_{c_n}\text{sign}(\dot{q}) \qquad \dot{q} < 0 \tag{C.1}$$

$$\tau_{vc}^{f}(t) = f_{v_p}\dot{q} + f_{c_p}\text{sign}(\dot{q}) \qquad \dot{q} > 0 \tag{C.2}$$

The corresponding fitted parameters are visible in table C.

joint	f_{v_p}	f_{c_p}	f_{v_n}	f_{c_n}
2	3.57	14.26	7.64	18.25
3	1.64	3.27	1.70	4.15
4	2.58	6.93	2.89	4.95
5	1.61	3.75	1.64	3.64
6	-	-	-	-
7	0.27	0.82	0.21	1.23

Table C.1: Friction compensation fit parameters.